Journal of Nuclear Materials 496 (2017) 41–53

Contents lists available at ScienceDirect

Journal of Nuclear Materials

journal homepage: www.elsevier.com/locate/jnucmat

Recrystallization and thermal shock fatigue resistance of nanoscale ZrC dispersion strengthened W alloys as plasma-facing components in fusion devices

Z.M. Xie [a], S. Miao [a, b], R. Liu [a], L.F. Zeng [a, b], T. Zhang [a, *], Q.F. Fang [a, b, **], C.S. Liu [a], X.P. Wang [a], Y.Y. Lian [c], X. Liu [c, ***], L.H. Cai [d]

[a] Key Laboratory of Materials Physics, Institute of Solid State Physics, Chinese Academy of Sciences, Hefei, Anhui 230031, China
[b] University of Science and Technology of China, Hefei, Anhui 230026, China
[c] Southwestern Institute of Physics, Chengdu, Sichuan 610041, China
[d] ATTL Advanced Materials Co., Ltd, Beijing, Beijing 100083, China

ARTICLE INFO

Article history:
Received 15 May 2017
Received in revised form
13 September 2017
Accepted 13 September 2017
Available online 18 September 2017

ABSTRACT

Recrystallization and thermal shock fatigue resistance behavior of nanoscale ZrC dispersion strengthened bulk tungsten alloys (W-0.5 wt% ZrC, WZrC) as potential candidates for plasma-facing components were investigated. By employing heat treatments with isochronal experiments, the evolution of the tungsten grain size/orientation, second phase particle distribution, thermal conductivity and mechanical properties were systematically studied. The effects of edge-localized mode like transient heat events on the as-rolled and recrystallized WZrC were investigated carefully. Pulses from an electron beam with durations of 1 ms were used to simulate the transient heat loading in fusion devices. The cracking thresholds, cracking mechanisms and recrystallization under repetitive (100 shots) transient heat loads were investigated. Results indicate that the cracking threshold of all the WZrC samples is 220–330 MW/m^2 (corresponding to a heat load parameter F = 7.0–10.4 MJ/$m^2s^{1/2}$) at room temperature and the heat bombardment induced recrystallization occurs at a heat parameter of 10.4 MJ/$m^2s^{1/2}$.

1. Introduction

Tungsten is selected as the prime candidate for plasma facing components (PFCs) for the divertor in the magnetic confinement nuclear fusion reactors of the International Thermonuclear Experimental Reactor (ITER), due to its melting temperature of 3410 °C, high thermal conductivity, high neutron load capacity, low tritium retention and low sputtering yield [1–5]. These superior properties all together are considered to have major impact on the component lifetime. In spite of these advantages, the selection of tungsten materials as PFCs is quite demanding, because the PFCs will be directly exposed to extreme conditions in the fusion plasma, such as high levels of neutron irradiation (3–30 dpa $year^{-1}$) [6], a high heat flux (HHF) of energetic particles [7], electromagnetic radiation, sputtering erosion and some severe events or scenarios like plasma disruptions, edge localized modes (ELMs) and vertical displacement events (VDEs). Especially in the VDEs, a heat flux of 10–100 MW/m^2 with duration of milliseconds to several hundred milliseconds was predicted [8]. The high energy stored in short periods on W materials leads to simultaneously high stress and surface temperatures which will alter the microstructure of tungsten materials by recrystallization and grain growth. Typically, recrystallization in W materials leads to the formation of new grain boundaries (GBs) with random orientations [9]. These random GBs in the unstable high-energy state are very susceptible to cracking and thus prone to fracture as referred to as recrystallization embrittlement. The recrystallization embrittlement causes significant degradation of material properties like a loss in mechanical strength [10], a decrease in fracture toughness [11] and an increase in the ductile-to-brittle-transition temperature (DBTT) [12].

Recently, some dispersion strengthened tungsten materials

* Corresponding author.
** Corresponding author. Key Laboratory of Materials Physics, Institute of Solid State Physics, Chinese Academy of Sciences, Hefei, Anhui 230031, China.
*** Corresponding author.
E-mail addresses: zhangtao@issp.ac.cn (T. Zhang), qffang@issp.ac.cn (Q.F. Fang), xliu@swip.ac.cn (X. Liu).

http://dx.doi.org/10.1016/j.jnucmat.2017.09.022
0022-3115/

have been developed and attracted more attention. For example, the small sized W-1.1%TiC fabricated by the grain boundary sliding-based microstructural modification (GSMM) exhibits very high fracture strength up to about 4.4 GPa and appreciable flexural ductility at room temperature (RT) [13]. However, the inferior fabrication efficiency as well as the small size of this GSMM W-TiC product would limit the engineering application as PFCs or divertors. In recent works, an interface designed bulk W-0.5 wt%ZrC alloy with hybrid microstructures was developed, which contains refined equiaxed sub-grains, elongated mother grains and well-dispersed nanoparticles [14]. This bulk W-ZrC alloy exhibits excellent mechanical properties, including a flexural strength of 2.5 GPa, a strain of 3% at RT and the DBTT of about 100 °C. In addition, it could sustain 3.3 MJ/m^2 thermal load without any cracks during single shot high heat flux tests with a pulse length of 5 ms using an electron beam [15]. But the recrystallization behavior and especially the thermal shock fatigue resistance of this ZrC dispersion strengthened W material have not been investigated, despite the importance of these parameters as mentioned above. Moreover, even less investigation of the particle distribution, mechanical properties and especially the corresponding thermal shock/fatigue resistance of these materials at different recrystallization levels (initial state, recovery state, partially recrystallized and fully recrystallized states) has been performed so far. However, these varied states should not be negligible for the lifetime and reliability of nuclear fusion reactor components, because the performance of different grades of tungsten under transient heat loads is strongly related to microstructures such as grain size, grain orientation and second phase particle distribution [16,17]. So it's quite important to study the performance of bulk W-ZrC alloys at different recrystallization states under ELM-like transient heat events.

In this work, the recrystallization behaviors and thermal shock fatigue resistance (during ELM-like transient heat events) of rolled bulk W-0.5 wt%ZrC alloy plates were systematically studied. Conventional heat treatments with isochronal experiments were applied to determine the recrystallization temperature and achieve the various recrystallized samples. The evolution of the tungsten grain size, grain orientation, second phase particles distribution, thermal conductivity and mechanical properties after recrystallization have been studied carefully. In addition, an electron beam with duration of 1 ms were applied to simulate the transient heat loading in fusion devices. The crack formation, patterns as well as the dynamic recrystallization and grain growth behaviors under the extreme condition of repetitive high stress and temperature during the electron beam loading were specifically investigated and analyzed.

2. Experimental details

2.1. Preparing materials

A schematic diagram of the experimental procedures is given in Fig. 1. W–0.5 wt%ZrC alloys (hereafter abbreviated as WZrC) were fabricated using pure W powders with particle size of sub-micrometer (purity>99.9% trace metals basis), and nano-sized ZrC powders (average particle size of 47 nm, purity>99%). A TEM image of the initial ZrC powder and the corresponding particle size distribution are shown in Fig. 2. The detailed fabrication process was described in the earlier work [14].

2.2. Experimental setup

As a first step towards understanding the recrystallization behavior of the rolled WZrC alloy, conventional heat treatments

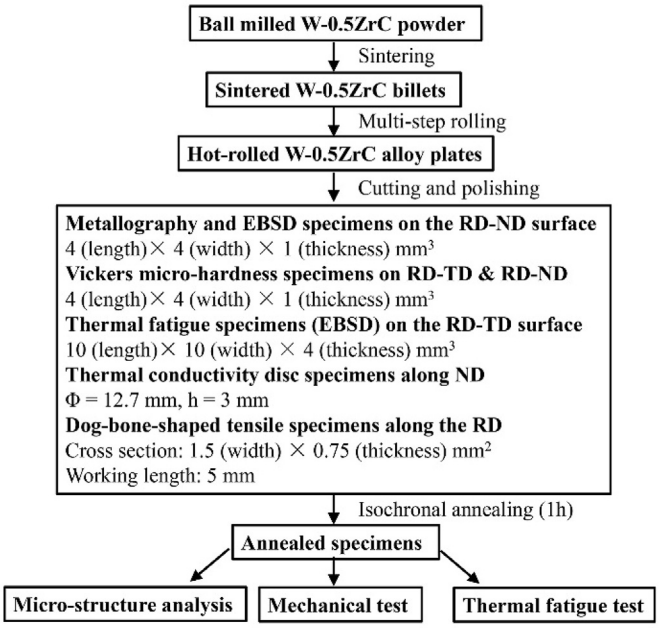

Fig. 1. A schematic diagram of experimental procedures.

with isochronal experiments were applied. The as-rolled WZrC plates were cut into several testing specimens with different sizes in certain directions as shown in Fig. 1. RD, TD and ND represent the rolling direction, transverse direction and normal direction, respectively. These specimens were polished with 2000 mesh SiC paper and then isochronally annealed at nine temperatures (1000 °C, 1100 °C, 1200 °C, 1300 °C, 1400 °C, 1500 °C, 1600 °C, 1700 °C and 1800 °C) for 1 h in vacuum. The heating and cooling rates were all 10 °C/min during the heat treatments. Hereafter, the annealed WZrC alloy is abbreviated as A-WZrC. For isochronal experiments, where annealing is carried out at various temperatures for a constant time, recrystallization is actually a microstructural transformation as a function of the changed annealing temperature (T_a). So the quantitative metallography analysis (the fraction of recrystallization) was adopted to describe the recrystallization states. In order to study the effect of recrystallization on the performance of WZrC alloys, the Vickers micro-hardness, tensile strength, thermal conductivity and especially the thermal shock fatigue resistance of these annealed specimens were also investigated.

Before Vickers micro-hardness tests, the annealed specimens cut from RD–ND and RD–TD surfaces were electrolytically polished in 2% sodium hydroxide aqueous solution at RT with a polishing voltage of 18 V and a current density about 3 mA/mm^2, to obtain the mirror-polished and stress-free surfaces. These polished specimens were then subjected to Vickers micro-hardness testing at RT with a load of 200 g and a dwell time of 15 s.

For tensile testing, the WZrC plates were cut into dog-bone specimens with a cross-section of 1.5 × 0.75 mm^2 and a working length of 5 mm, and then mechanically polished to remove the cutting-induced scratches and other defects. The as-rolled and annealed tensile specimens were all along the rolling direction. The tensile tests were carried out using an Instron-5967 machine using a constant speed of 0.06 mm/min at various temperatures from RT to 500 °C.

The thermal conductivity (γ) was calculated from the thermal diffusivity (α), density (ρ) and specific heat (C_p) according to the relation $\gamma = \alpha C_p \rho$. The α was determined using the laser flash

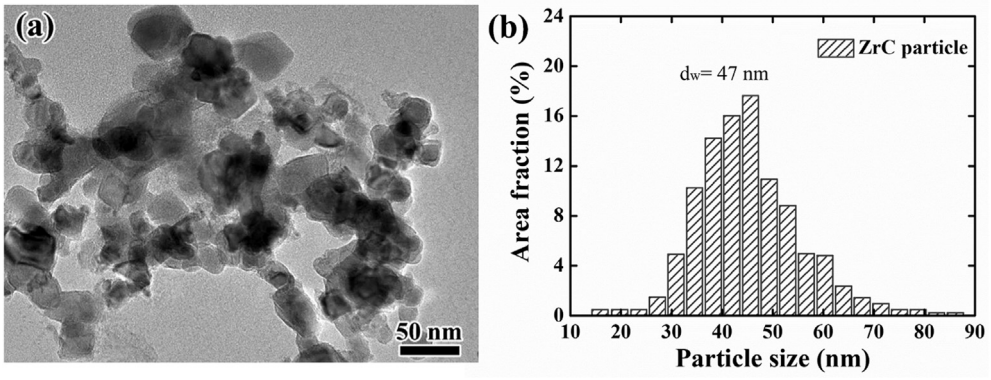

Fig. 2. A TEM image of (a) the initial ZrC powder and the statistical result showing (b) the corresponding particle size distribution.

diffusivity system (LFA457 Micro flash, NETZSCH). The C_p was measured by a thermal analyzing apparatus (Dupont 1090B, USA). The density ρ was measured by the Archimedes methods. The room temperature properties are listed in Table 1.

High heat flux tests were performed on the RD-TD surface using the electron beam device EMS–60 (60 kW Electron-beam Material-test Scenario) at Southwestern Institute of Physics, China. This device provides an electron beam with a maximum power of 60 kW [18]. The acceleration voltage of electron beam is in the range of 90–150 kV. The maximum electron current is 400 mA. In this experiment, a Gaussian shaped electron beam with a focused diameter of approximately 1 mm (FWHM) and an acceleration voltage of 120 kV was used. The beam was scanned across the surface (scanning area 4×4 mm^2) with a frequency of 31 kHz in x-direction and 40 kHz in y-direction, respectively. The used absorption coefficient for tungsten was ~0.55, which corresponds to the value obtained by means of Monte-Carlo simulations [19], and is in agreement with the reported experimental data [20]. According to the previous works [15], the threshold power density for melting of rolled W-ZrC alloys was estimated to be around 0.88 GW/m^2 for 5 ms. Therefore, in this study, two different absorbed power densities (APD, 0.22 and 0.33 GW/m^2), well below the melting threshold, were selected to investigate the cracking regime and dynamic recrystallization of the as-rolled and recrystallized WZrC alloys by multiple shots up to 100 with a single pulse duration of 1 ms. Heat loads were applied using the heat load parameter F, which was directly proportional to the surface power load multiplied by the square root of the pulse duration. The corresponding heat parameters were 7.0 MJ/m^{2}s$^{1/2}$ (0.22 GW/m^2) and 10.4 MJ/m^{2}s$^{1/2}$ (0.33 GW/m^2), respectively. The based temperature (T_0) of the bulk specimens for thermal shock tests was kept constant at RT. The inter-pulse time was 3 s to allow a complete cooldown of the specimens to RT after each individual pulse.

2.3. Characterization

The metallography was obtained using an optical microscope (ZEISS-AX10) after polishing and etching (10% potassium ferricyanide with 10% sodium hydroxide aqueous solution). More elaborated metallographic images of the thermal loaded area on specimens were obtained using field emission scanning electron microscopy (FESEM, SU8020 Hitachi). Electron Backscatter Diffraction Pattern (EBSD) mappings were measured with an acceleration voltage of 20 kV and collected using a CRYSTAL detector (Oxford Instruments, Oxfordshire, UK) equipped on a Zeiss SIGMA FESEM to characterize the microstructure of specimens after electrolytic polishing in 5% sodium hydroxide aqueous solution with a constant voltage of 11 V and a current density of 3 mA/mm^2. The EBSD images were slightly filtered through a software (HKL Tango) to eliminate the influences of second-phase particles on tungsten grain observations. The EBSD shows the orientation and distribution of tungsten grains and the corresponding misorientation angle. For the isochronally annealed WZrC specimens, EBSD examinations were carried out on the RD–ND surface. To further characterize the tungsten grain size and orientation evolution after the extreme thermal shock loads, the scanning area on the RD–TD plane were also measured. TEM specimens were prepared by twin-jet in a Struers Tenupol-5. The second phase particle size was statistically analyzed using quantitative metallography based on 500 particles from TEM images of the as-rolled and annealed WZrC specimens.

3. Results and discussion

3.1. Recrystallization of the hot rolled WZrC

Thermal stability of the hot rolled bulk WZrC alloy was studied by annealing for 1 h from 1000 to 1800 °C. The metallographic images of the RD-ND plane before and after annealing are presented in Fig. 3. Intuitively, two different tungsten grains appeared in the metallographic graphs: fine elongated grains (high resolution images are shown in Fig. 4(a)) with grey appearance and large equiaxed grains with bright appearance. Almost all grains maintained the elongated shape when T_a was below 1300 °C. With further increasing the T_a, the proportion and aspect ratio of these elongated grains decreased significantly until 1600 °C, as depicted

Table 1
Room-temperature properties of the as rolled and annealed WZrC.

Materials	Density (10^3 kg/m^3)	Specific heat (J/kg·K)	Thermal diffusivity (10^{-6} m^2/s)	Thermal conductivity (W/m·K)
As rolled WZrC	19.07	131	60.2	150
1100 °C A-WZrC	19.08	130	60.3	150
1400 °C A-WZrC	19.09	130	60.8	153
1500 °C A-WZrC	19.1	131	62.3	156
1600 °C A-WZrC	19.1	130	64.8	161

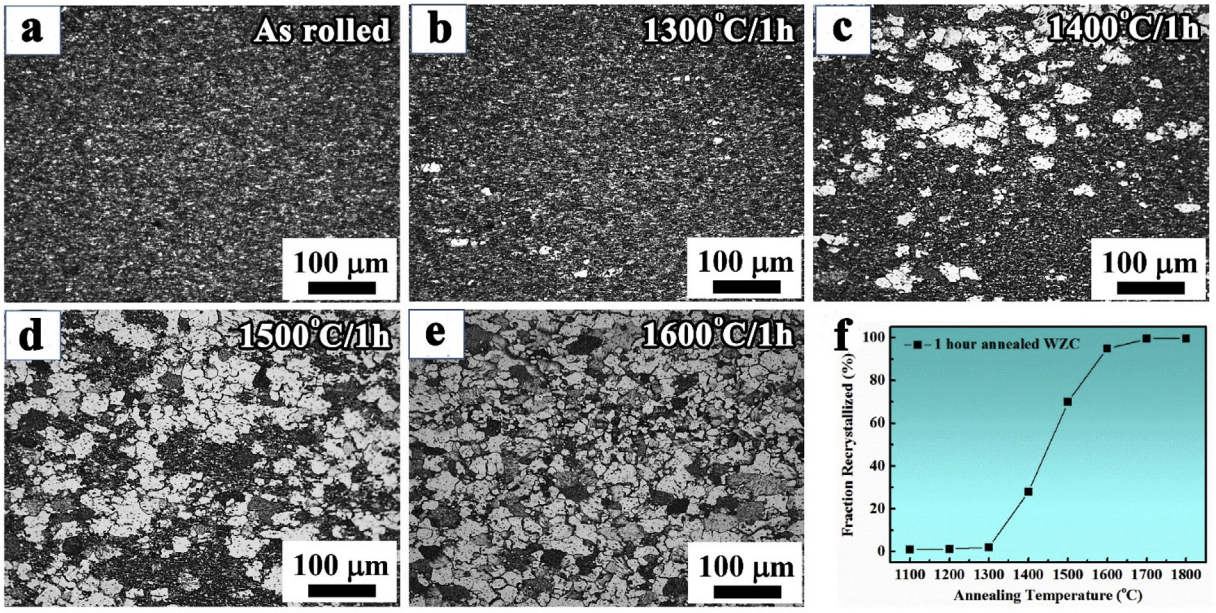

Fig. 3. Optical micrographs of the (a) as-rolled, (b–e) annealed WZrC and (f) the recrystallization fraction versus the T_a after treatment for 1 h.

in Fig. 3(a)–(e). On the other hand, large equiaxed grains appeared after annealing at 1300 °C, indicating the start of recrystallization. The fraction of large equiaxed grains increased rapidly with further increasing T_a from 1300 °C to 1600 °C as indicated by the statistical results in Fig. 3(f). Especially, when the T_a was up to 1600 °C, the initial elongated tungsten grains were almost replaced by the large equiaxed grains (Fig. 3(e)), suggesting the full recrystallization. Defining the recrystallization temperature as the starting temperature at which deformed materials undergo a microstructural transformation like nucleation and/or grain growth, here the recrystallization temperature of the hot rolled WZrC alloys is 1300 °C.

In order to get a more detailed view of grains and to analyze the texture, an electron microscope with an EBSD detector was used. Definition of colors and directions is as follows: red refers to <001>, green <101> and blue <111>. In Fig. 4, the x–y plane represents the RD–ND and the x-direction is the rolling direction. The z-direction is the transverse direction perpendicular to the observation plane. Definition of the GBs is as follows: tungsten grains with misorientation angle ($\theta > 10°$) are indicated by the black thick line and with misorientation angle ($2° < \theta < 10°$) are indicated by the grey thin line.

It could be clearly seen in Fig. 4(a), that the mother-grains were elongated along the rolling direction and about 15 μm in length and 4 μm in width, corresponding to an aspect ratio of about 3.8. The elongated mother-grains in the rolled WZrC alloy were composed of fine equiaxed sub-grains. The inverse-pole figure of the as-rolled sample shows that in most areas the rolling direction is parallel to the [101] direction, suggesting a strong [101] texture. The EBSD result of 1400 °C A-WZrC is shown in Fig. 4(b). Some large equiaxed grains with size ranging from 7 to 50 μm have been observed which suggest that partial recrystallization and grain growth occurred during 1400 °C annealing. In addition, the grain orientation mainly maintained [101] direction parallel to the rolling direction, except for a weak [113] texture parallel to the y direction (ND). Further increasing the T_a to 1600 °C, the rolled WZrC alloys underwent drastic recrystallization and grain growth, resulting in large amounts of coarsening grains (7–80 μm) by exhausting initial elongated tungsten grains. In addition, an obvious [001] texture were developed along the normal direction, as shown in Fig. 4(c).

In this work, only grains with misorientation angles $\theta > 2°$ were measured. In this case the average tungsten grain sizes were calculated as ~1.41 μm (in the as-rolled WZrC), ~3.92 μm (in the 1400 °C/1 h annealed WZrC) and ~11.7 μm (in the 1600 °C A-WZrC), as shown in Fig. 5(a)–(c), respectively. It can be seen that about 83% grains are less than 3.5 μm in the as-rolled WZrC specimen (as shown in Fig. 5(a)). However, only 20% grains are less than 3.5 μm in the 1400 °C A-WZrC because of the partial recrystallization and grain growth (Fig. 5(b)). In the 1600 °C A-WZrC, the size of all grains ranges from 7 to 80 μm (Fig. 5(c)), as a result of the full recrystallization. The statistical distributions of the grain misorientation angle before and after recrystallization are shown in Fig. 5(d). As indicated by the black line in Fig. 5(d), the grains with low misorientation angle (2° to 10°) are dominant in the as-rolled WZrC. In the 1400 °C A-WZrC, there is a bimodal misorientation distribution which contains two main parts: one is the remained low angle part and another is the relatively high angle part near 50° as depicted by the red dotted line in Fig. 5(d). This newly developed high angle part came from the recrystallized large grains. After full recrystallization in the 1600 °C A-WZrC, the distribution of grain misorientation obeys the Mackenzie curve based on the random distribution of grain orientation.

Further TEM analysis gives more detailed information on the evolution of microstructures and second phase particle distributions as shown in Fig. 6. In the as-rolled WZrC, the size distributions of the particles (nano ZrC particles) shown in Fig. 6(a) (right panel) indicate that ZrC particles have an average size of 51 nm and a size range from 10 to 160 nm. Lots of tangled dislocations in tungsten grain interior or near the GBs were observed in the as-rolled WZrC as indicated by the blue arrows in Fig. 6(a) (left panel). It is well known that deformation energy is stored in materials mainly in the form of dislocations [21,22]. The stored energy in the deformed WZrC alloy could be released in three main processes: recovery, recrystallization, and grain coarsening. Typically, recovery processes involve the rearrangement of dislocations to lower their energy like dislocations of opposite sign climbing towards one another [21]. In the 1300 °C A-WZrC, the dislocation density was decreased in comparison with the as-rolled one as shown in

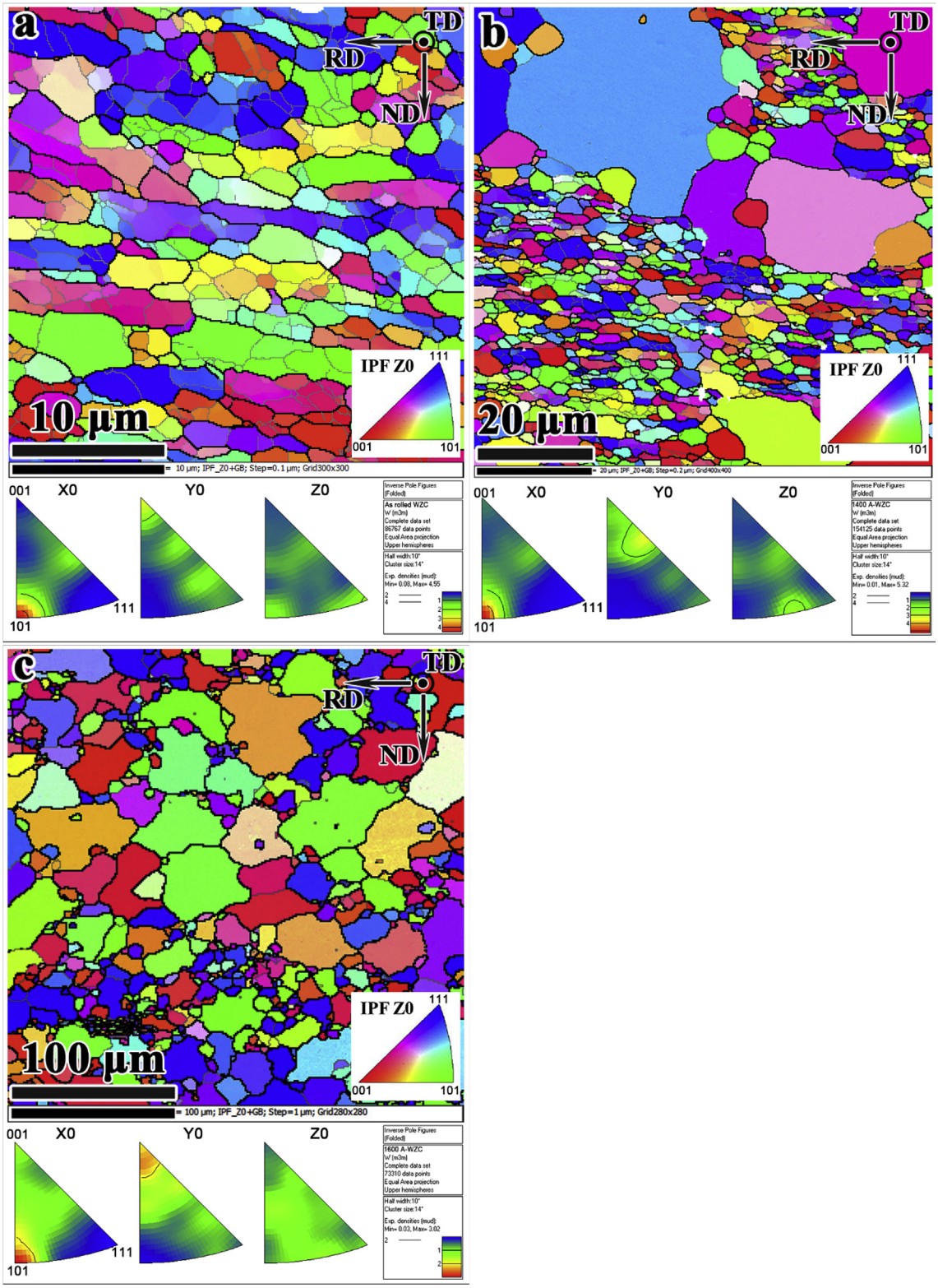

Fig. 4. EBSD Characterization of the (a) as rolled, (b) 1400 °C/1 h and (c) 1600 °C/1 h annealed WZrC alloys.

Fig. 6(b) (left panel), which resulted from the recovery process. On the other hand, the ZrC particle distribution in the 1300 °C/1 h annealed sample kept the same with the unannealed one: the size range from 20 to 150 nm and the average size about 53 nm. As indicated by the above metallography and EBSD analysis, the rolled WZrC underwent recrystallization and grain growth during 1400 °C/1 h and 1600 °C/1 h annealing. Actually, recrystallization is the formation and migration of high angle grain boundaries driven by the stored energy [23]. This grain boundary migration during recrystallization may drive the second phase particle migration and

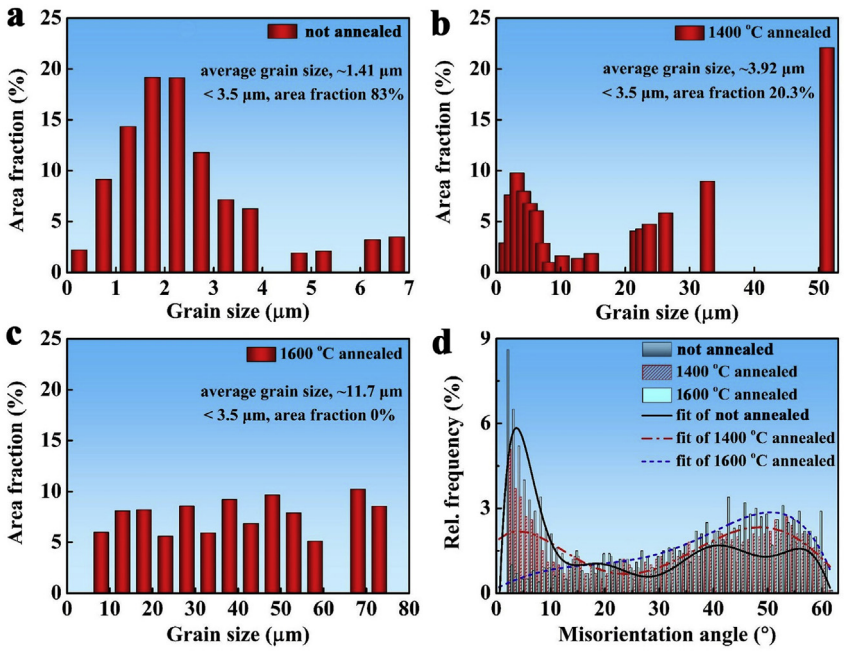

Fig. 5. The tungsten grain size distributions in the (a) as rolled, (b) 1400 °C/1 h and (c) 1600 °C/1 h annealed WZrC alloys and (d) the misorientation distribution before and after recrystallization.

thus cause particle aggregation and coarsening as indicated by the red circle line in Fig. 6(c) and (d). So the average particle size increased to 64 nm and 66 nm in the 1400 °C A-WZrC and 1600 °C A-WZrC, respectively. Especially, in the case of 1600 °C/1 h annealed sample, full recrystallization and rapid grain coarsening further increased the grain boundary migration and the expense of initial small grains, resulting in almost all large grains and coarsened second particles (~180 nm) within the tungsten grain as indicated by the blue arrows in Fig. 6(d).

3.2. Mechanical properties before/after recrystallization

The Vickers micro-hardness of the as-rolled WZrC is 510 HV for RD-ND plane and 506 HV for RD-TD plane, respectively. The isotropic hardness may result from the equiaxed sub-grain geometry in the as-rolled WZrC. It is well known that the hardness is closely related to the microstructure, therefore the recrystallization behavior can be further reflected by the evolution of hardness with T_a. From the plotting shown in Fig. 7, two characteristic temperatures of 1300 °C and 1600 °C divide this curve into three stages including i) the recovery stage for 1000 °C < T_a < 1300 °C, ii) the partial recrystallization stage for 1300 °C < T_a < 1600 °C and iii) the full recrystallization and grain growth stage for T_a > 1600 °C. In the recovery stage, the hardness of annealed WZrC samples is about 490 HV which is just 4% lower than that of the as-rolled one. And this value changes slowly with increasing the T_a (<1300 °C), which mainly comes from the stable structure as indicated by the above EBSD/TEM analysis and depicted by the sketch map in Fig. 7 (upper left). However, in the partial recrystallization stage, the hardness decreases abruptly with increasing T_a from 1300 °C to 1600 °C which comes from the explosive increasing number of recrystallized large grains and reduction of fine sub-grains (as shown in Fig. 3(f)), as depicted by the sketch map in Fig. 7 (upper middle). After the full recrystallization at 1600 °C, the hardness reaches a minimum value of about 400 HV and keeps constant with increasing the T_a to 1700 °C or 1800 °C, which is 21% smaller than that of the initial value. The corresponding sketch map of grain structures after full recrystallization is shown in Fig. 7 upper right.

Recrystallization induced degradation of strengthen and ductile to brittle transition (referred to a higher DBTT) is a very important issue for the candidate first wall materials. Fig. 8 shows the annealing temperature dependence of tensile engineering stress–strain curves of rolled WZrC alloys. It can be seen that all the WZrC samples show typical brittle fracture at RT but a detectable plastic deformation at 100 °C, indicating a ductile to brittle transition in the range from RT to 100 °C. Defining the DBTT as the lowest temperature at which a sample undergoes a minimum elongation >0 without failure [24], here the DBTT of all the WZrC samples studied are about 100 °C. This DBTT value is lower than that of the pure tungsten (400 °C) specified by ITER [25] and some reported tungsten materials like rolled pure W (~200 °C from the 3-point bend test) [26], hot forged W–2Y_2O_3 (~200 °C from the 3-point bend test) [27], swaged/rolled W-1.0La_2O_3 (~700 °C from the Charpy impact test) [28] and forged/rolled W–0.2TiC (~165 °C from the 3-point bend test) [29]. In addition, the tensile elongations (from 100 °C to 500 °C) of samples at different stages such as recovery, partial recrystallization and even full recrystallization have all been increased compared with the as-rolled one (as shown in Figs. 8 and 9(b)), suggesting an improved plasticity. The unchanged DBTT combining with the increased plasticity implies an improved ductility induced by recrystallization. This is surprising because, normally, recrystallization leads to embrittlement due to the formation of random grain boundaries with high energy which are very susceptible to cracking and are prone to fracture. The formation of these weak boundaries was frequently attributed to the segregation and re-precipitation of gaseous interstitial elements of oxygen and/or nitrogen which are insoluble in the W matrix [9]. However, in the case of our ZrC dispersion strengthened W materials, it has been confirmed that active element Zr, decomposed from ZrC, could capture impurity oxygen in tungsten and form stable ZrO_x particles during sintering [14], which would undoubtedly reduce the detrimental oxygen concentration in GBs and thus mitigate recrystallization embrittlement.

In order to clearly present the evolution of tensile properties

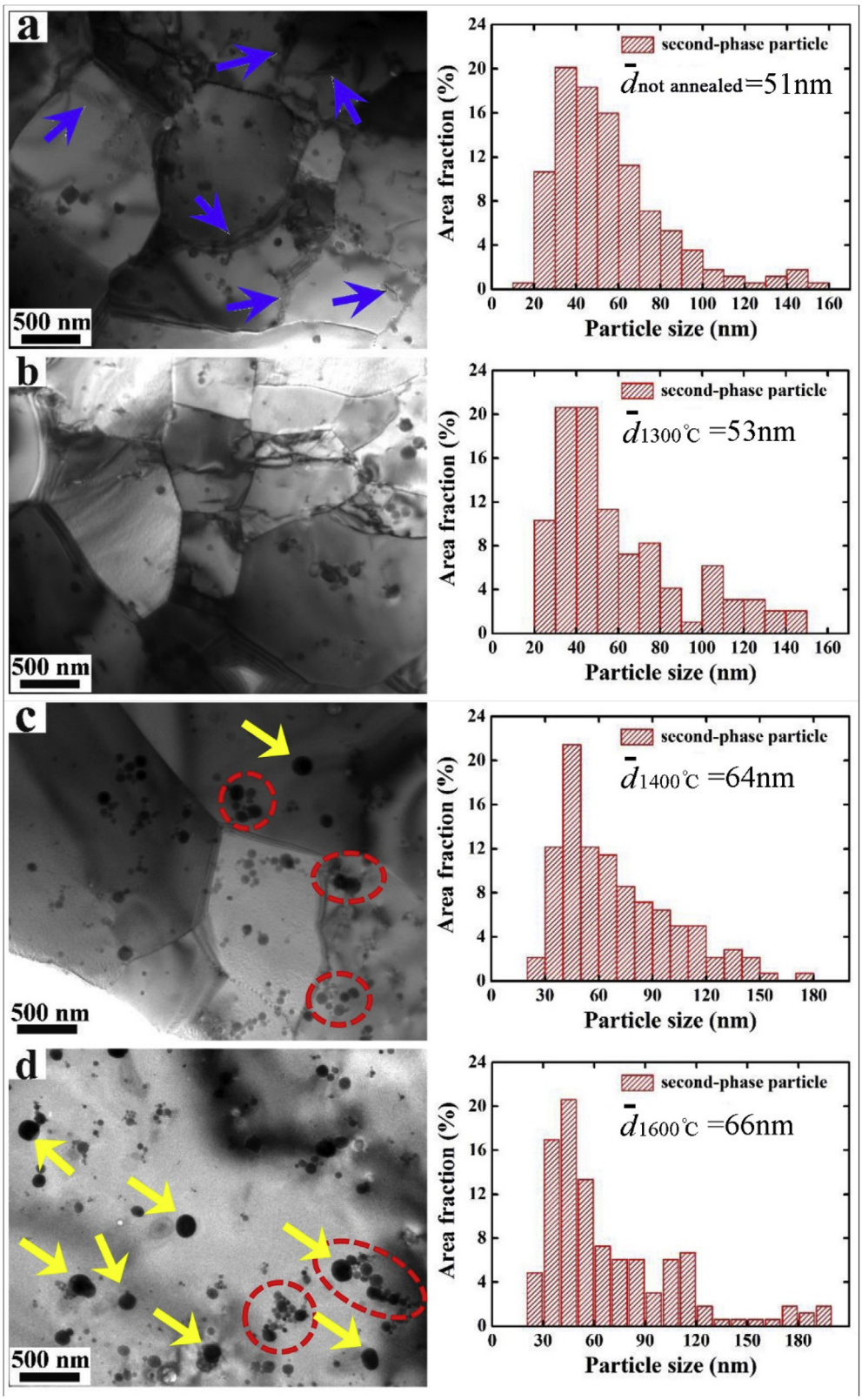

Fig. 6. TEM images showing the microstructure and dispersed particles (left) and statistical results showing the corresponding particle size distribution (right) in the (a) as rolled, (b) 1300 °C/1 h, (c) 1400 °C/1 h and (d) 1600 °C/1 h annealed WZrC alloys.

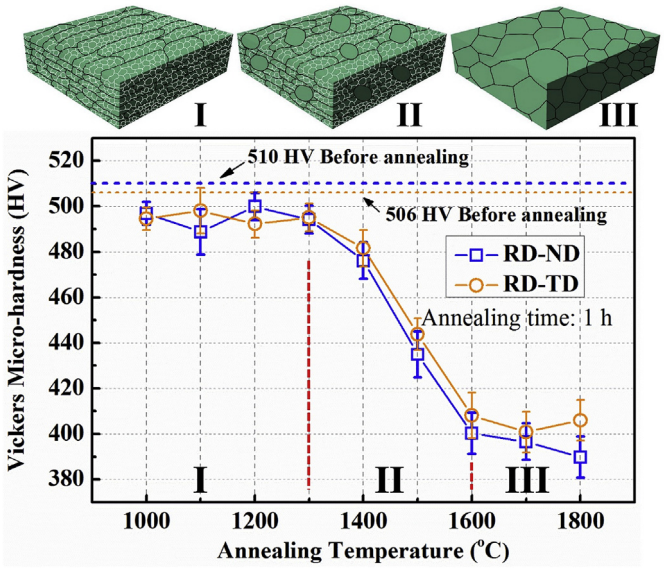

Fig. 7. Vickers micro-hardness and tungsten grain structure (sketch maps) evolutions after annealing for 1 h at temperatures between 1000 and 1800 °C. The horizontal dotted lines indicate the hardness of the as-rolled WZrC before annealing. I) the recovery stage, II) the partial recrystallization stage and III) the full recrystallization and grain growth stage.

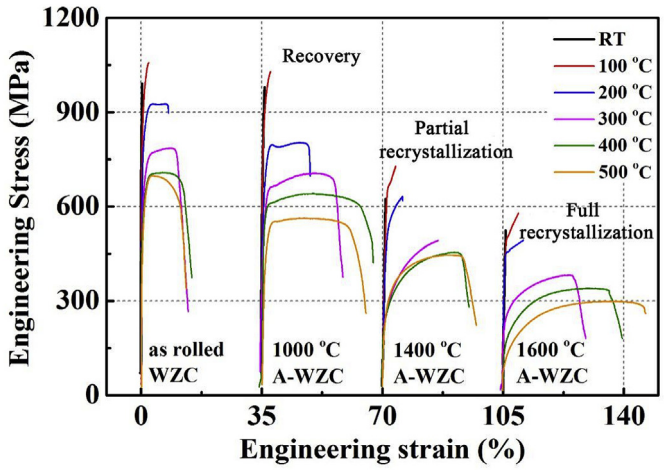

Fig. 8. Tensile behaviors of the as rolled, 1000 °C/1 h (recovery), 1400 °C/1 h (partial recrystallization) and 1600 °C/1 h (full recrystallization) annealed WZrC alloys at temperatures between RT and 500 °C.

with the T_a, the ultimate tensile strength (UTS) and total elongation (TE) are shown as a function of test temperature in Fig. 9, where the result of rolled pure W [30] is also presented for comparison. It can be clearly seen that at RT the UTS value of the as-rolled WZrC is 990 MPa, about 80% higher than that of rolled pure W (550 MPa) [30]. From 100 °C to 500 °C, the UTS values of the as-rolled WZrC are always 200 MPa higher than that of the rolled pure W (as shown in Fig. 9(a)). While for TE, the as-rolled WZrC performed better than the rolled pure W when the testing temperature was below 200 °C. But at 300 °C, 400 °C and 500 °C, the as-rolled WZrC exhibited limited elongations of all about 10%. This limited plasticity may come from the high density of defects like tangled dislocations which would introduce stress concentrations and become the possible sites of crack initiation. After recovery treatments, especially annealed at 1000 °C, the high-temperature elongation

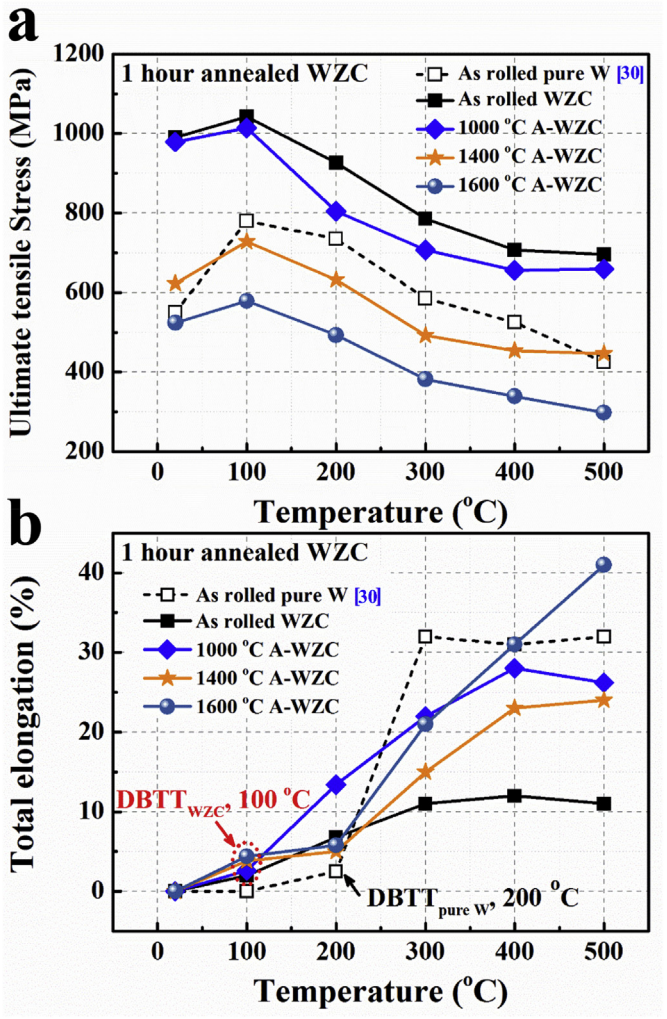

Fig. 9. The UTS (a) and elongation (b) of the as rolled and annealed WZrC alloys at different temperatures, note that values of the reported pure W [30] are present for comparison.

increased from 10% to 22%, 28% and 27% at 300 °C, 400 °C and 500 °C (as shown in Fig. 9(b)), respectively. The UTS values of the 1000 °C A-WZrC decreased slightly in comparison with the as-rolled one, which still kept higher than 650 MPa from RT to 500 °C (as shown in Fig. 9(a)). That's to say, an appropriate recovery annealing is important, which could effectively enhance the toughness of the rolled WZrC alloys. However, the partial and/or full recrystallization significantly decreased the UTS (for example at RT, from 990 MPa to 491 MPa) as shown in Figs. 8 and 9(a), which was mainly attributed to the weak coarsened tungsten grains. These coarsened grains with low strength are easy to crack through a typical transgranular fracture under a high tensile load. This fracture type will be discussed in the following thermal shock fatigue behavior section in more details.

3.3. Thermal conductivities before/after annealing treatments

The thermal conductivity is also important for first wall materials, which will influence the capacity of steady high thermal loads. So it is necessary to investigate the effect of recrystallization on thermal conductivity. Fig. 10 shows the evolution of the thermal conductivities of the rolled WZrC alloys with annealing temperature, where the values of a W grade fulfilling the ITER specifications

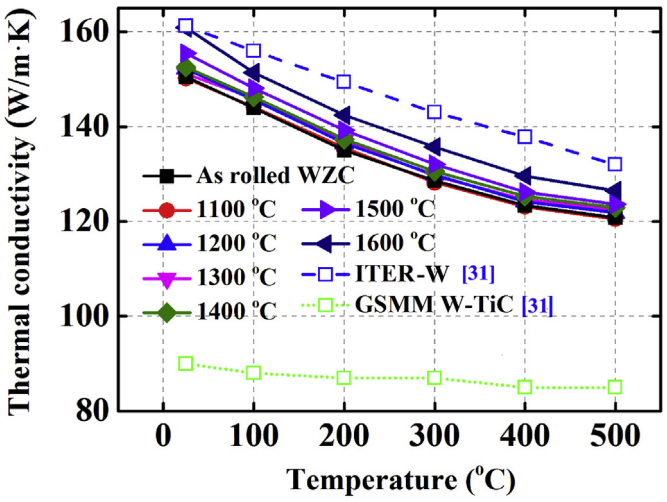

Fig. 10. Thermal conductivities of the as rolled and annealed WZrC samples, note that values of the reported ITER-W and GSMM W-TiC [31] are also present for comparison.

(ITER-W) and GSMM W-TiC alloy [31] are also presented for comparison. The thermal conductivity of the as-rolled WZrC reduced slowly with the increasing temperature and kept larger than 120 W/m·K from RT to 500 °C, which was 44% higher than that of the GSMM W-TiC alloy, but about 15 W/m·K lower than that of the ITER-W. This phenomenon probably resulted from the much more GBs, ZrC/W phase boundaries and other defects like point defects and dislocations than those in pure W, but much less than those in the GSMM W-TiC alloy. These defects significantly enhanced the scattering on electrons/phonons and therefore reduced the thermal conductivity, which on the other hand suggests that the thermal conductivity could be increased through reducing the defects. As can be seen in Fig. 10 and Table 1, the thermal conductivities of annealed WZrC alloys have indeed been increased slightly with increasing the T_a from 1100 °C to 1600 °C.

3.4. Thermal shock fatigue behavior

In order to investigate the material response to transient heat load events, the as-rolled and recrystallized WZrC samples were all tested by repetitive (100 shots in total) electron beam loading at RT. Fig. 11 is a low magnification SEM image of the loaded surface after 100 shots with the heat parameter of 7.0 MJ/m^{2}s$^{1/2}$. No cracks and no surface roughening were detected for both the as-rolled and annealed samples, which means that WZrC alloys could sustain this heat bombardment without any surface damages. When the heat parameter was increased to 10.4 MJ/m^{2}s$^{1/2}$ (100 shots), cracks were observed on the heat loaded sample surfaces as shown in Fig. 12. The finite element analysis results indicated that the crack formation can be mainly attributed to thermal tensile stresses induced by temperature gradients perpendicular to the heated surface during the heat off [32,33]. Usually, during heating, temperature gradients induce compressive stress and result in plastic and/or elastic deformation as shown in Fig. 13(a). When the tensile stress generated during the cooling stage is larger than the tensile strength of the WZrC alloy, the cracks will form, as shown in Fig. 13(b). For the as-rolled specimens, five main cracks propagated straightly through the loaded area with a direction parallel to the RD as shown in Fig. 12(a). After recovery annealing at 1000 °C or 1300 °C, the cracks were still in the straight form but have lower cracking densities compared to the as-rolled one (as shown in Fig. 12(b) and (c)). The reduced cracking density may came from the improved toughness as well as the decreased residue stresses in the recovery-annealed WZrC as discussed in the above microstructure and mechanical sections. In the case of partially recrystallized sample (1400 °C annealed), dendritic cracking appeared as shown in Fig. 12(d), which indicated the existence of different cracking propagation way between the 1400 °C A-WZrC and the as-rolled or recovery-annealed specimens. With increasing the recrystallization fraction, such as for the 1500 °C A-WZrC sample, the dendritic cracks increased and constructed a dense crack network covering the entire electron beam loaded area (as shown in Fig. 12(e)), which implied that the cracking propagation was closely related to recrystallized grains. For the fully recrystallized WZrC sample (Fig. 12(f)), more dense crack networks were observed. But the sides (cracks) of this network looked more homogeneous and circumferential.

In order to further explore the mechanism of the different cracking patterns, the loaded surfaces with cracks have been investigated carefully. Fig. 14 presents the higher magnification of surface damages/cracks on the as-rolled, partially and fully recrystallized samples, where the original surface of the as-rolled sample before heat bombardment is also present. It can be clearly seen that the as-rolled WZrC consisted of fine equiaxed sub-grains (<3.5 μm) as indicated by the above EBSD analysis. The SEM image clearly exhibits that these straight cracks on the as-rolled WZrC are primary intergranular cracks with jagged shape and crack width of ~5 μm. This cracking pattern suggests that the strength of the fine equiaxed sub-grains is larger than that of the GBs and thus cracks propagate along the GBs. In the case of partially recrystallized sample (1500 °C annealed), the dendritic cracks were initiated in the recrystallized large grains and then spread along GBs with crack width of ~5 μm, which potentially resulted from the relatively low strength of these recrystallized grains. For the 1600 °C A-WZrC specimen with dense crack networks, the cracks spread along GBs of the fully recrystallized grains with crack width of ~3.5 μm. That's to say, the boundaries of the recrystallized grains were weaker than grain matrixes. So it is emphasized again that strengthening GBs is important for enhancing the thermal shock resistance as well as the mechanical properties.

The repetitive (100 shots) high heat flux loading on the tungsten surface could form high stress and temperature simultaneously. These extreme conditions may lead to the dynamic recrystallization and grain growth and thus influence the thermal fatigue resistance of the PFC. In order to study the recrystallization and grain growth in the as-rolled and annealed WZrC alloys after the repetitive high heat parameter of 10.4 MJ/m^{2}s$^{1/2}$ (APD, 330 MW/m^2), EBSD examinations were carried out. Definition of colors and directions in Fig. 15 is as follows: red refers to <001>, green <101> and blue <111>. The x–y plane represents the RD–TD and the x-direction is the rolling direction. The z-direction is the normal direction out of the observation plane. Fig. 15(a)–(c) show the EBSD results of the as-rolled, 1400 °C and 1600 °C annealed WZrC specimens after 100 shots, respectively. Intuitively, a straight crack along the RD was observed in the as-rolled WZrC (as shown in Fig. 15(a)), which was consistent with the above SEM analysis. In addition, the inverse-pole figure (Fig. 15(a) bottom panel) presents two preferred orientations after repetitive thermal loads: one is the original [101] direction parallel to the RD and the other is a newly developed crystal orientation of [111] direction parallel to the ND. This newly developed tungsten grain orientation suggested the occurrence of recrystallization induced by the repetitive high stress and temperature. Due to the breakdown of the single color infrared pyrometer used for measuring the surface temperature of the samples in electron beam test facility EMS-60, we had to theoretically calculate the surface temperatures by using the following formula [34,35]:

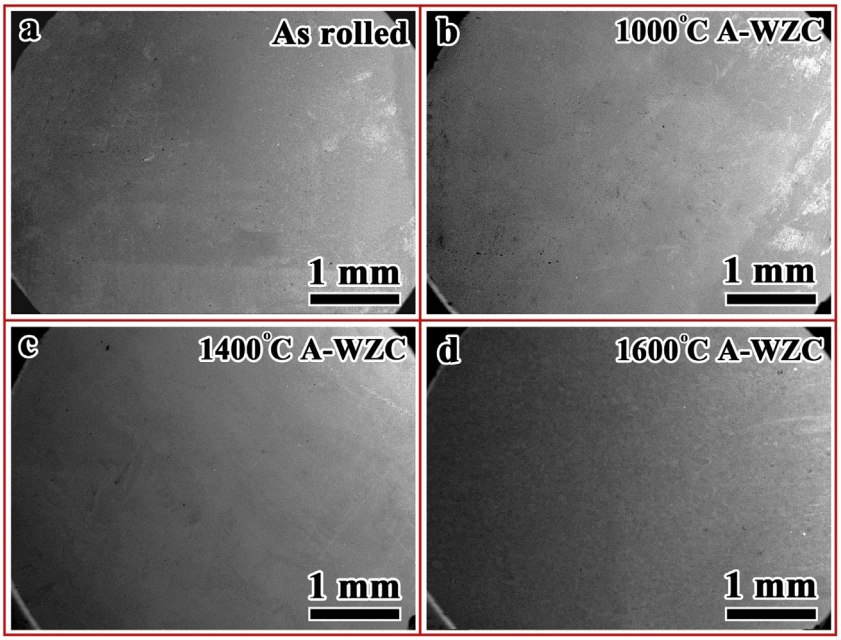

Fig. 11. Low magnification SEM images showing the loaded areas on the (a) as rolled, (b) 1000 °C/1 h, (c) 1400 °C/1 h and (d) 1600 °C/1 h annealed WZrC samples after 100 shots with the heat flux of 7.0 MJ/m^{2}s$^{1/2}$.

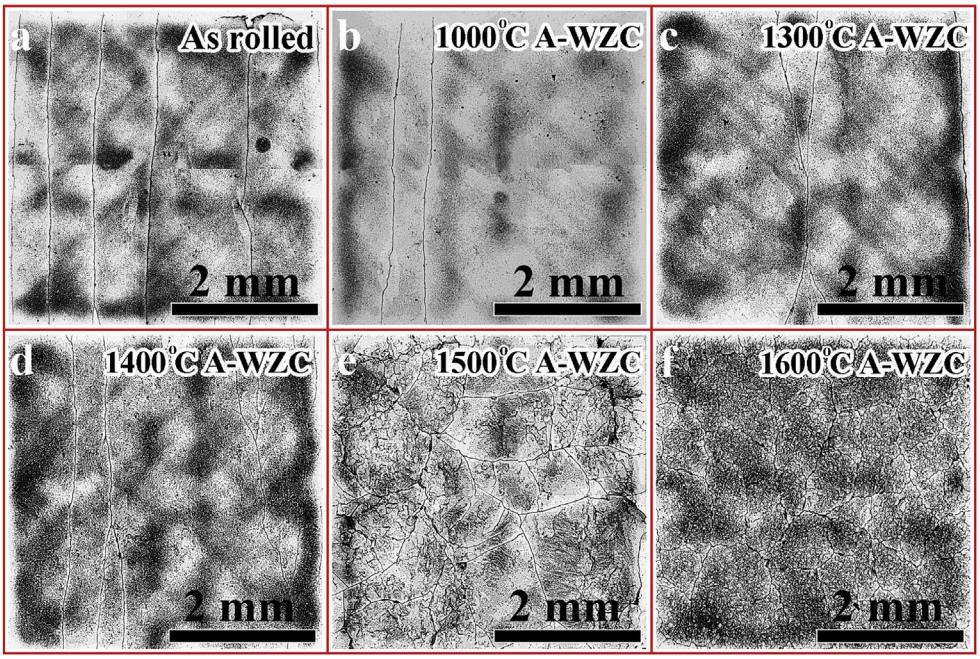

Fig. 12. Surface morphologies showing cracks in the loaded areas on the as rolled and annealed WZrC samples after 100 shots with the heat flux parameter of 10.4 MJ/m^{2}s$^{1/2}$.

$$T_{max} = T_0 + 2P\left(t/\pi\gamma\rho C_p\right)^{1/2} \quad (1)$$

where T_{max} stands for the maximum surface temperature due to a transient high heat load, T_0 for the based temperature at RT, P for the power density (W/m^2), t for pulse duration (s), γ for the thermal conductivity (W/m·K), ρ for the density (kg/m^3) and C_p for the specific heat (J/(kg·K). When we took the values of C_p, γ and ρ for the rolled WZrC at RT (as shown in Table 1), it was found that the threshold power density for melting of the WZrC lies around 0.82 GW/m^2 for 5 ms, which is consistent with the previous work (0.66–0.88 GW/m^2) [15]. This theoretical calculation has been indicated a valid method to simulate the maximum surface temperature especially in the relatively low power density [36]. So in this work, the maximum surface temperatures of the as-rolled WZrC was calculated to be about 633 °C at 330 MW/m^2 for 1 ms at a single shot, which is obviously below the recrystallization temperature tested by the isochronal experiment. It could be concluded that the recrystallization in the as-rolled WZrC was due to the repeatedly dual acceleration of the high stress and

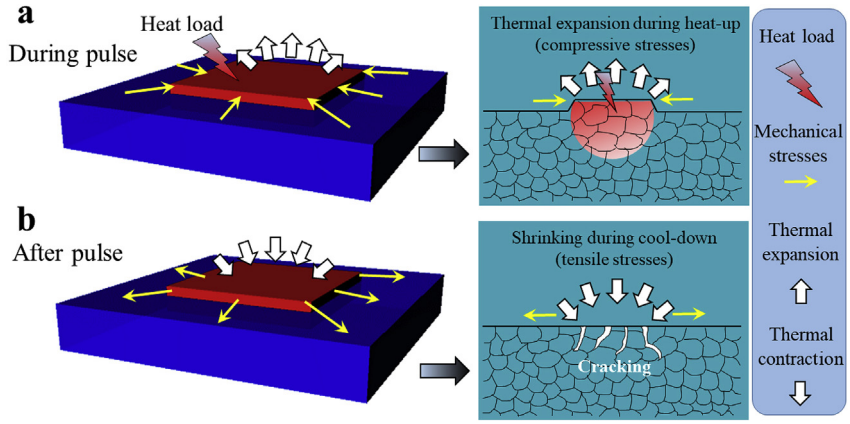

Fig. 13. Sketch maps showing the general mechanism of crack formation in thermal loading tests.

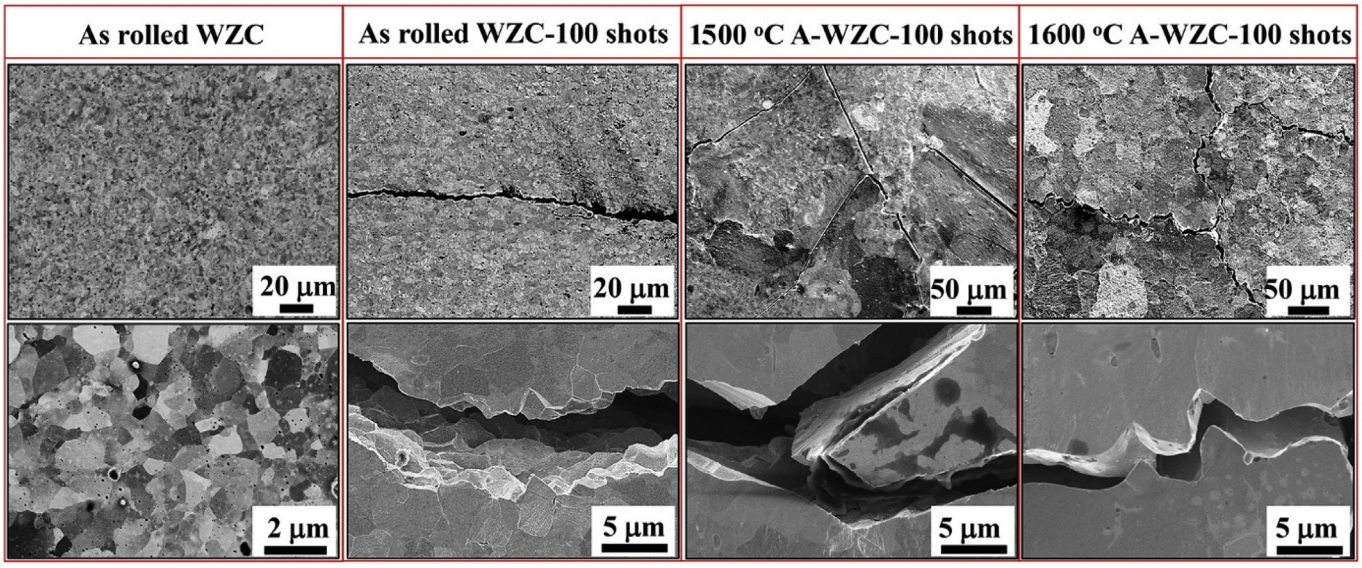

Fig. 14. High magnification SEM images showing the different cracking patterns in the as rolled, 1500 °C/1 h (partially recrystallized) and 1600 °C/1 h (fully recrystallized) treated WZrC alloys after 100 shots with the heat flux of 10.4 MJ/m^{2}s$^{1/2}$. The metallographic graphs of the as rolled WZrC before thermal shock tests are presented for comparison.

temperature. Normally, the stress could be released through plastic deformation like surface roughening during the heating stage if the thermally induced compressive stresses exceed the yield strength of the tungsten. But this surface roughness has not been observed in the as-rolled WZrC samples after repetitive thermal loads with the heat flux parameter of 7.0–10.4 MJ/m^{2}s$^{1/2}$, which suggests that the stress is only consumed by elastic deformation. This behavior also implied the high yield strength of the as-rolled WZrC alloys. In this case, the loading stress would be accumulated in material surfaces in the form of stored energies like dislocations. The gradually increased dislocations may introduce stress concentrations and become the possible sites of crack initiation which would result in a weak thermal fatigue resistance (100 shots, cracking threshold 220–330 MW/m^2, almost the same with the performance of the ITER-W [37]) in comparison with the reported excellent thermal shock resistance (single shot, 660–880 MW/m^2) of the as-rolled WZrC [15]. On the other hand, the stored energy may promote the recrystallization and thus reduce the recrystallization temperature to a relatively low value during the repetitive thermal loads [38]. The repetitive high heat flux induced recrystallization has also been confirmed by long-pulse laser beam loading experiments in the cold-rolled tungsten [39].

In order to further confirm the occurrence of recrystallization in the annealed WZrC, the EBSD results of the 1400 °C and 1600 °C A-WZrC after thermal loads are present in Fig. 15(b) and (c), respectively. As shown in Fig. 15(b), some newly developed tungsten crystals with [113] orientation parallel to the RD and parts of them with [113] orientation parallel to the TD were observed in the 1400 °C A-WZrC, which deviated from the original preferred grain orientation of [101] parallel to the RD. In the case of 1600 °C A-WZrC, only a strong [001] texture along the ND was developed from the initial (001)[101] texture after thermal loads. That's to say, repetitive high heat flux loading on the tungsten surface indeed led to the recrystallization and the preferred orientation of these recrystallized grains is related to the initial state of materials.

The material damage was also investigated from the top surface to the bulk of the flat disc shaped blocks using optical image analyses of polished and etched cross-section surfaces as shown in Fig. 16. It can be seen that the cracking depth were all about 230 μm for the as-rolled and annealed WZrC after 100 shots with the high heat parameter of 10.4 MJ/m^{2}s$^{1/2}$. And in the 1400 °C A-WZrC, an thermal influenced area (depth ~ 500 μm) with large grains (~100 μm) was very different from the bottom area (grain size about several microns), which should come from the

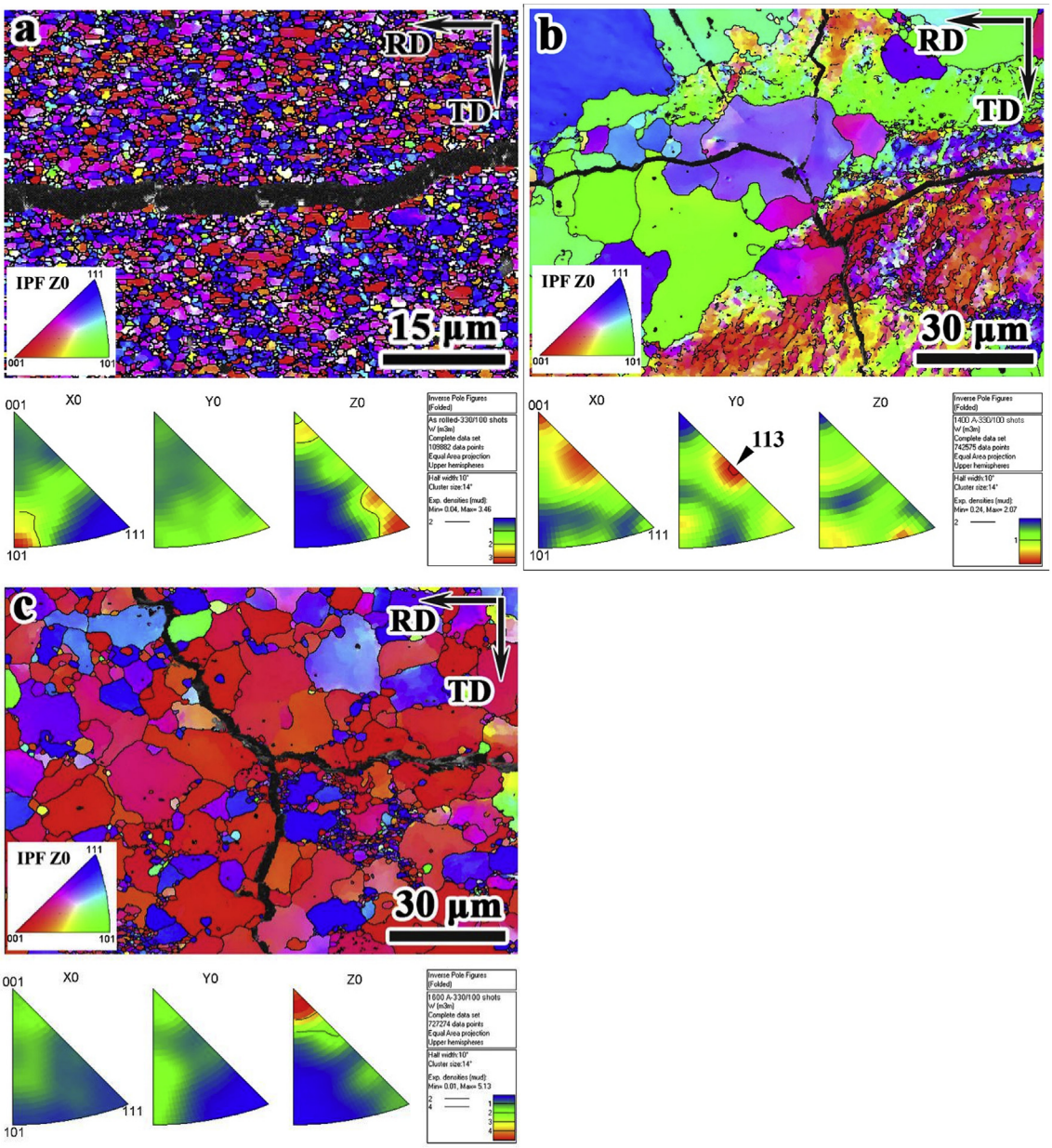

Fig. 15. EBSD Characterization of the loaded areas on the (a) as rolled, (b) 1400 °C/1 h and (c) 1600 °C/1 h annealed WZrC alloys after 100 shots with the heat flux of 10.4 MJ/m^{2}s$^{1/2}$.

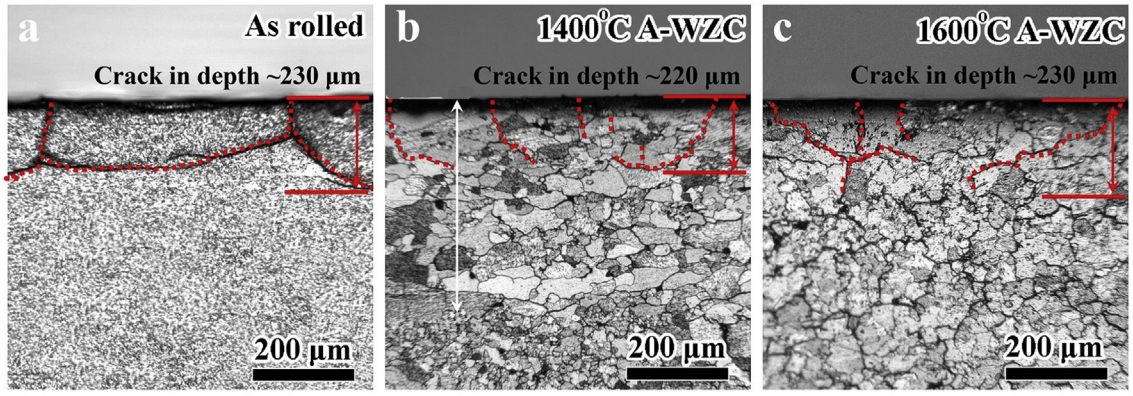

Fig. 16. Optical images showing the cracking depth on the cross-section surfaces of the (a) as rolled, (b) 1400 °C/1 h and (c) 1600 °C/1 h annealed WZrC alloys after 100 shots with the heat flux of 10.4 MJ/m^{2}s$^{1/2}$.

recrystallization near the surface region.

4. Conclusion

This work has focused on understanding the recrystallization behaviors as well as physics processes and underlying mechanisms involved in thermal shock fatigue issues for W-0.5 wt%ZrC alloys under transient heat loads. Recrystallization behaviors of the rolled bulk WZrC alloy have been investigated using conventional heat treatments with isochronal experiments, which indicates the starting temperature of recrystallization for the hot rolled WZrC alloys is 1300 °C. In addition, the evolution of the tungsten grain size/orientation, second phase particle distribution, thermal conductivity and mechanical properties after different annealing treatments has been studied systematically. It is found that recovery annealing could improve the toughness and thermal conductivity of the rolled WZrC alloys without reducing the strength or changing the tungsten grain structure/orientation and second phase particle distribution/size.

The effect of transient thermal loads (100 shots at RT) on the as-rolled and annealed WZrC alloys have been investigated by employing an electron beam test facility (EMS-60). It is found that the cracking thresholds for the as-rolled and recrystallized WZrC samples are 220–330 MW/m^2 (F = 7.0–10.4 MJ/m^{2}s$^{1/2}$) at room temperature with 100 shots. Straight cracks with cracking width of ~5 μm and depth of ~230 μm were observed on the as-rolled and recovery-annealed WZrC sample surfaces. While dense crack networks with cracking width of 3–5 μm and depth of ~230 μm were found on the partially and fully recrystallized WZrC sample surfaces. The EBSD analysis shows that the heat bombardment could induce recrystallization on the WZrC sample surface at a heat parameter of 10.4 MJ/m^{2}s$^{1/2}$ and the preferred orientation of these recrystallized grains is related to the initial state of materials. It could be concluded that this heat loading induced recrystallization comes from the dual acceleration of the high stress and temperature. However, more plasma material interaction studies are needed to confirm the recrystallization mechanism and identify reliable materials for PFCs in reactor conditions.

Acknowledgements

This work was financial supported by the National Magnetic Confinement Fusion Program (with Grant No. 2015GB112000) and the National Natural Science Foundation of China (with Grant Nos. 11575241, 11374299, 51301164, 11375230, 51671184, 11274305 and 11475216).

References

[1] J. Knaster, A. Moeslang, T. Muroga, Nat. Phys. 12 (2016) 424–434.
[2] Q.Y. Huang, Y.C. Wu, J.G. Li, et al., J. Nucl. Mater 386–388 (2009) 400–404.
[3] Z. Dong, Z.Q. Ma, Y.C. Liu, et al., Sci. Rep. 7 (2017) 6051.
[4] V. Philipps, J. Nucl. Mater 415 (2011) S2–S9.
[5] R. Neu, R. Dux, A. Kallenbach, et al., Nucl. Fusion 45 (2005) 209–218.
[6] N. Baluc, K. Abe, J.L. Boutard, Nucl. Fusion 47 (2007) S696–S717.
[7] R.P. Wenninger, M. Bernert, T. Eich, et al., Nucl. Fusion 54 (2014) 114003.
[8] Y. Yuan, H. Greuner, B. Böswirth, et al., J. Nucl. Mater 433 (2013) 523–530.
[9] H. Kurishita, H. Arakawa, S. Matsuo, et al., Mat. Trans. 54 (2013) 456–465.
[10] W. Guan, S. Nogami, M. Fukuda, et al., Plasma Fusion Res. 10 (2015), 1405073–1405073.
[11] D. Terentyev, J. Riesch, S. Lebediev, et al., Int. J. Refract. Mater. Hard Mater 66 (2017) 127–134.
[12] Y. Yuan, H. Greuner, B. Böswirth, et al., J. Nucl. Mater 433 (2013) 523–530.
[13] H. Kurishita, S. Matsuo, H. Arakawa, et al., J. Nucl. Mater 398 (2010) 87–92.
[14] Z.M. Xie, R. Liu, S. Miao, et al., Sci. Rep. 5 (2015) 16014.
[15] Z.M. Xie, R. Liu, S. Miao, et al., J. Nucl. Mater 469 (2016) 209–216.
[16] A. Suslova, O. El-Atwani, S.S. Harilal, et al., Nucl. Fusion 55 (2015) 033007.
[17] Y. Yuan, B. Xu, B.Q. Fu, et al., Nucl. Fusion 54 (2014) 83026.
[18] Y. Lian, X. Liu, Z. Cheng, et al., J. Nucl. Mater 455 (2014) 371–375.
[19] M. Wirtz, J. Linke, G. Pintsuk, et al., J. Nucl. Mater 438 (2013) S833–S836.
[20] X. Zhang, Q. Yan, J. Nucl. Mater 444 (2014) 428–434.
[21] R.D. Doherty, D.A. Hughes, F.J. Humphreys, et al., Mat. Sci. Eng. A 238 (1997) 219–274.
[22] W. Guo, S.K. Li, F.C. Wang, et al., Scr. Mater 60 (2009) 329–332.
[23] F.J. Humphreys, Acta Mater 45 (1997) 4231–4240.
[24] A. Wronski, A. Foukdeux, J. Less Common Met. 8 (1965) 149–158.
[25] X. Liu, Y. Lian, L. Chen, et al., J. Nucl. Mater 463 (2015) 166–169.
[26] V. Krsjak, S.H. Wei, S. Antusch, et al., J. Nucl. Mater 450 (2014) 81–87.
[27] M. Battabyal, R. Schäublin, P. Spätig, et al., Mat. Sci. Eng. A 538 (2012) 53–57.
[28] Q. Yan, X. Zhang, T. Wang, et al., J. Nucl. Mater 442 (2013) S233–S236.
[29] Y. Ishijima, S. Kannari, H. Kurishita, et al., Mat. Sci. Eng. A 473 (2008) 7–15.
[30] T. Shen, Y. Dai, Y. Lee, J. Nucl. Mater 468 (2016) 348–354.
[31] G. Pintsuk, H. Kurishita, J. Linke, et al., Phys. Scr. T145 (2011) 014060.
[32] I.E. Garkusha, I. Landman, J. Linke, et al., J. Nucl. Mater 415 (2011) S65–S69.
[33] J. Linke, T. Loewenhoff, V. Massaut, et al., Nucl. Fusion 51 (2011) 073017.
[34] Y. Kikuchi, I. Sakuma, D. Iwamoto, et al., J. Nucl. Mater 438 (2013) S715–S718.
[35] T. Hirai, G. Pintsuk, Fusion Eng. Des. 82 (2007) 389–393.
[36] M. Zhao, Z. Zhou, M. Zhong, et al., J. Nucl. Mater 470 (2016) 236–243.
[37] M. Wirtz, J. Linke, Th. Loewenhoff, et al., Transient heat load challenges for plasma-facing materials during long-term operation, https://doi.org/10.1016/j.nme.2016.12.024.
[38] A. Rollett, F.J. Humphreys, G.S. Rohrer, et al., Recrystallization and Related Annealing Phenomena, Elsevier, 2004.
[39] A. Suslova, O. El-Atwani, D. Sagapuram, et al., Sci. Rep. 4 (2014) 06845.